



Universiteit
Leiden
The Netherlands

Binding kinetics of ZM241385 derivatives at the human adenosine A(2A) receptor

Guo, D.; Xia, L.; Veldhoven, J.P.D. van; Hazeu, M.D.; Mocking, T.; Brussee, J.M.; ... ; Heitman, L.H.

Citation

Guo, D., Xia, L., Veldhoven, J. P. D. van, Hazeu, M. D., Mocking, T., Brussee, J. M., ... Heitman, L. H. (2014). Binding kinetics of ZM241385 derivatives at the human adenosine A(2A) receptor. *Chemmedchem*, 9(4), 752-761. doi:10.1002/cmdc.201300474

Version: Publisher's Version

License: [Licensed under Article 25fa Copyright Act/Law \(Amendment Taverne\)](#)

Downloaded from: <https://hdl.handle.net/1887/3209420>

Note: To cite this publication please use the final published version (if applicable).

DOI: 10.1002/cmdc.201300474

Binding Kinetics of ZM241385 Derivatives at the Human Adenosine A_{2A} Receptor

Dong Guo, Lizi Xia, Jacobus P. D. van Veldhoven, Marc Hazeu, Tamara Mocking, Johannes Brussee, Adriaan P. IJzerman, and Laura H. Heitman^{*[a]}

Classical drug design and development rely mostly on affinity- or potency-driven structure–activity relationships (SAR). Thus far, a given compound's binding kinetics have been largely ignored, the importance of which is now being increasingly recognized. In the present study, we performed an extensive structure–kinetics relationship (SKR) study in addition to a traditional SAR analysis at the adenosine A_{2A} receptor (A_{2A}R). The ensemble of 24 A_{2A}R compounds, all triazolotriazine derivatives resembling the prototypic antagonist ZM241385 (4-(2-((7-

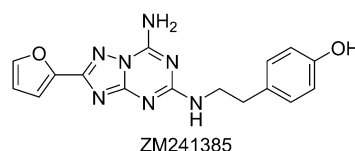
amino-2-(furan-2-yl)-[1,2,4]triazolo[1,5-*a*][1,3,5]triazin-5-yl)amino)ethyl)phenol), displayed only minor differences in affinity, although they varied substantially in their dissociation rates from the receptor. We believe that such a combination of SKR and SAR analyses, as we have done with the A_{2A}R, will have general importance for the superfamily of G protein-coupled receptors, as it can serve as a new strategy to tailor the interaction between ligand and receptor.

Introduction

G protein-coupled receptors (GPCRs) are among the largest and most heavily investigated drug targets in the drug research community. Traditional early phase drug design and discovery campaigns of GPCRs largely depend on equilibrium affinity- or potency-based structure–activity relationships (SAR). This approach of lead optimization allows a quick synthesis–evaluation feedback loop to pool abundant candidate compound assemblies for further drug evaluation. Nevertheless, this classical SAR approach does not seem to predict clinical efficacy very well, which is evidenced by the high levels of attrition during the translation of lead compound in vitro activity into in vivo and clinical evaluation. To address this issue, several recent reviews have emphasized the importance of binding kinetics, and in particular, the lifetime of a drug–target binary complex (i.e., drug–target residence time (RT)), as a critical differentiator and predictor for drug efficacy and safety.^[1] In addition to the RT, the association rate of a ligand–receptor interaction, which reflects the “target engagement time” (ET), should also be taken into consideration in the early phases of drug research. This is especially important for designing drugs that require a fast onset of action and potentially for drugs that act on temporarily existing targets, such as protein–protein interactions.^[2] Therefore, an extensive structure–kinetics relationship (SKR) investigation, in addition to the traditional SAR anal-

ysis, can be of great use in the early phases of candidate drug optimization.

The human adenosine A_{2A} receptor (A_{2A}R) is a subtype of adenosine receptors (other subtypes are A₁, A_{2B}, and A₃) belonging to the superfamily of GPCRs.^[3] Antagonists for this receptor have been reported as potential treatment for Parkinson's disease.^[4] As such, many compounds with high A_{2A}R affinities have been developed,^[5] including the reference antagonist ZM241385 (4-(2-((7-amino-2-(furan-2-yl)-[1,2,4]triazolo[1,5-*a*][1,3,5]triazin-5-yl)amino)ethyl)phenol), a triazolotriazine deriva-



tive.^[6] These compounds were well characterized and optimized in terms of their binding affinity and thus benchmarked for later medicinal chemistry attempts targeting the A_{2A}R. For example, Vu and colleagues synthesized ZM241385 derivatives with increased bioavailability.^[7] However, the success rate of the developed A_{2A}R antagonists in clinical trials is disappointingly low. On one hand, this indicates that the results of currently used preclinical animal models do not translate well into clinical studies. On the other hand, traditional, affinity-directed SAR alone may not be sufficient enough to select candidates for preclinical tests, especially when comparing compounds that are otherwise biologically or chemically similar. Although A_{2A}R antagonists have been previously investigated extensively in terms of their affinity or potency, little is known about their binding kinetics thus far. It is of great importance to be able to optimize the kinetic profiles of such compounds, in addition to

[a] D. Guo, L. Xia, J. P. D. van Veldhoven, M. Hazeu, T. Mocking, Dr. J. Brussee, Prof. A. P. IJzerman, Dr. L. H. Heitman
Division of Medicinal Chemistry
Leiden Academic Centre for Drug Research (LACDR)
P.O. Box 9502, 2300 RA Leiden (The Netherlands)
E-mail: l.h.heitman@lacdr.leidenuniv.nl

Supporting information for this article is available on the WWW under <http://dx.doi.org/10.1002/cmdc.201300474>.

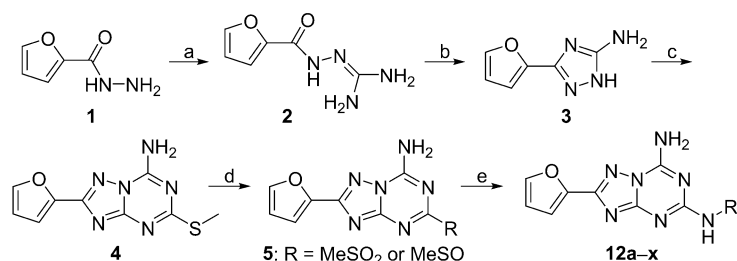
their affinity, by medicinal chemistry efforts. Thus, we decided to further extend the series of ZM241385 derivatives by progressively modifying the C₂ position to generate an insight into both SKR and SAR. We believe that the present study adds knowledge to our current understanding of drug design and development for A_{2A}R antagonists. Hopefully, this methodology of combining both SKR and SAR can be generally applied to other drug targets as well in the future.

Results and Discussion

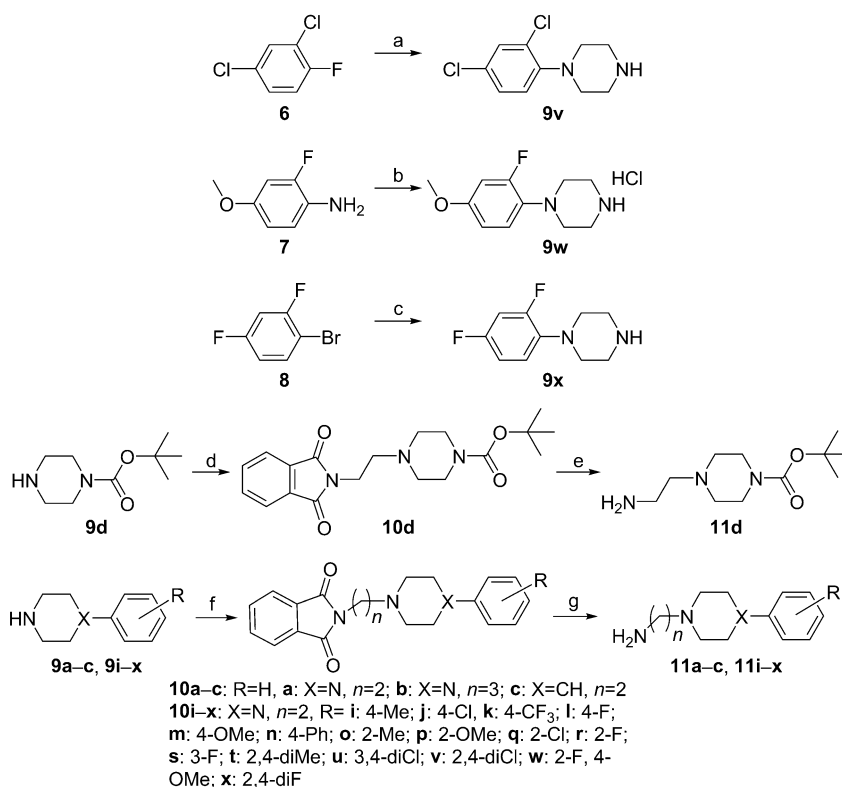
Chemical synthesis

Synthesis routes are depicted in Schemes 1 and 2. In total, an ensemble of 24 triazolotriazine derivatives (**12a–x**) was obtained. Notably, compounds **12a**, **12b**, and **12x** were previously reported by Vu et al.^[7c] and were re-synthesized in the present study, although using a different synthetic approach. All compounds (**12a–x**) were synthesized beginning from furan-2-carbohydrazide (**1**) to generate 7-amino-2-(furyl)-5-methylthio[1,2,4]triazolo[1,5-*a*][1,3,5]triazine (**4**), following the synthetic approach reported by Dolzhenko et al. and Jörg et al.^[8] Subsequently, **4** was oxidized with 3-chloroperbenzoic acid (*m*CPBA) to afford the corresponding sulfoxide/sulfone mixture **5**,^[9] which was substituted with a variety of commercially available amines (**11f–h**) to generate **12f–h**, or with in-house prepared amines (**11a–d** and **11i–x**) to generate **12a–d** and **12i–x**. Compound **12e** was obtained by the N-Boc deprotection of **12d**.

For the preparation of intermediate amines **11a–d** and **11i–x**, synthetic routes are depicted in Scheme 2. In brief, reactions



Scheme 1. General synthesis route to 24 triazolotriazine derivatives. *Reagents and conditions:* a) S-methylisothiourea sulfate (2:1), 4% NaOH(aq), room temp.; b) H₂O, room temp.; c) 1. (MeS)₂C=NCN, heat, 180 °C; 2. CH₂Cl₂/CH₃OH (2:1), reflux; d) *m*CPBA (70% strength), CH₂Cl₂, 0 °C → room temp.; e) Et₃N, CH₃CN.



Scheme 2. Preparation of key intermediates. *Reagents and conditions:* a) piperazine, *N,N*-dimethylacetamide, 165 °C; b) bis(2-chloroethyl)amine hydrochloride, Na₂CO₃, 130 °C, butanol; c) *t*BuONa, BINAP, Pd₂(dba)₃, toluene, N₂, 110 °C; d) K₂CO₃, NaI, butanone, reflux; e) H₂NNH₂·H₂O, EtOH; f) 3-bromoalkylphthamide, K₂CO₃, DMF, 70 °C; g) H₂NNH₂·H₂O, EtOH, 70 °C.

were carried out via N-alkylation of the commercially available piperazine derivatives (**9a–d** and **9i–u**) or the in-house synthesized phenylpiperazines (**9v–x**), which were derived from **6–8**,^[10] to obtain the appropriate N-phthalimide-protected alkyl piperazines (**10a–d** and **10i–x**). This was followed by deprotection of the phthalimide to afford the free amines (**11a–d** and **11i–x**).

SAR and SKR of triazolotriazine derivatives

The SAR and SKR analyses were initiated by testing two compounds, **12a** and **12b**, then chemical modifications were gradually introduced to these two compounds (Table 1). Several observations were made: 1) the molecule with a two-carbon spacer was superior to the compound with a three-carbon spacer. The former (**12a**, $K_i = 0.30 \pm 0.08$ nM; RT = 164 ± 32 min) displayed a fourfold higher affinity and 41-fold longer RT than the latter (**12b**, $K_i = 1.3 \pm 0.1$ nM; RT = 4 ± 1 min). Such variation in linker length also resulted in different association rates (**12a**, $k_{on} = 0.051 \pm 0.005$ nM⁻¹·min⁻¹; **12b**, $k_{on} = 0.16 \pm 0.06$ nM⁻¹·min⁻¹). 2) Upon different degrees of C₂-phenylpiperazine modification, the ligand affinities were moderately to largely affected, while their receptor RT values were drastically shortened (**12d–h**), except for the Boc-protected intermediate **12d**. This compound, in fact, had a 30- and 20-fold improved

Table 1. Binding affinities and kinetics of ZM241385 and **12a–h**.

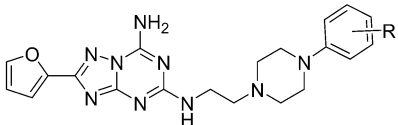
Compd	R	hA _{2A} R			hA ₁ R	
		K _i [nM] ^[a]	k _{on} [nM ^{−1} min ^{−1}] ^[b]	k _{off} [min ^{−1}] ^[b]	RT [min] ^[c]	K _i [nM]
ZM241385		0.40 ± 0.03	0.13 ± 0.06	0.014 ± 0.003	71 ± 21	255 ^[23]
12a		0.30 ± 0.08	0.051 ± 0.005	0.0061 ± 0.0020	164 ± 32	8% ^[d]
12b		1.3 ± 0.1	0.16 ± 0.06	0.25 ± 0.01	4 ± 1	30% ^[d]
12c		3.8 ± 0.8	0.20 ± 0.1	0.35 ± 0.03	3 ± 1	22% ^[d]
12d		1.5 ± 0.1	0.030 ± 0.003	0.012 ± 0.004	83 ± 17	2% ^[d]
12e		45 ± 0.1	0.0063 ± 0.0030	0.24 ± 0.10	4 ± 1	10% ^[d]
12f		31 ± 6	0.0057 ± 0.0020	0.25 ± 0.10	4 ± 1	11% ^[d]
12g		8.1 ± 0.5	0.046 ± 0.020	0.24 ± 0.10	4 ± 1	21% ^[d]
12h		64 ± 1	0.020 ± 0.002	0.62 ± 0.08	2 ± 0	32% ^[d]

[a] Displacement of specific [³H]ZM241385 binding from the hA_{2A}R at 4 °C. [b] k_{on} and k_{off} values were determined in a competition association assay at 4 °C. [c] RT (residence time) = 1/k_{off}. [d] Percent displacement of specific [³H]DPCPX binding from the hA₁R at 1 μM at 25 °C. Data are the mean ± SEM of three separate experiments, each performed in duplicate.

affinity and RT, respectively, relative to its truncated analogue (**12e**). Moreover, ET values were also significantly influenced by chemical modifications on the phenylpiperazine moiety. Specifically, **12g** displayed the fastest association rate (0.046 ± 0.020 nM^{−1}·min^{−1}). (3) Receptor RT values of **12a** or **12d** highlight the preference for an electron-withdrawing effect at the piperazine amine moiety. The insertion of an additional carbon into **12a** (between the piperazine and the phenyl group; **12g**) reversed the electron-withdrawing effect to a donating effect, which resulted in decreased A_{2A}R affinity (8.1 ± 0.5 nM) and RT (4 ± 1 min). Replacement of the nitrogen by a carbon atom on the “right side” of the piperazine (compare **12a** and **12c**) resulted in strongly decreased RT values that further confirmed the importance of the nitrogen in maintaining A_{2A}R affinity and RT (Table 1, Figure 1 for **12c**). Notably, the ET and RT of **12c** were the shortest for this series of compounds (except for the nearly 20-fold lower-affinity compound **12h**) without a large compromise on affinity. Taken together, these results highlight the importance of the C₂-phenylpiperazine-ethyl group, and more specifically show that the electron-deficient nitrogen (on the right side of the piperazine) has a role in preserving a tight ligand–receptor interaction.

The SAR and SKR were further analyzed with 16 phenyl-substituted **12a** analogues (Table 2, **12i–x**). Upon *para* substitution at the phenyl ring (**12i–n**), no significant change in ligand affinity (K_i values < 1 nM) was observed, except for **12n**, which had a 4.7-fold decrease in affinity (1.4 ± 0.2 nM). This decrease was probably caused by steric hindrance induced by the bulky phenyl substituent, which presumably also limited its RT to 29 ± 2 min and decreased the association rate to 0.018 ± 0.002 nM^{−1}·min^{−1}. In contrast, the other *para*-substituted compounds (**12i–m**) displayed a similar duration of in vitro receptor occupancy as ZM241385 (RT = 71 ± 21 min). In comparison with the convergent results upon *para*-position modifications, *ortho*-substituted analogues (**12o–r**) displayed divergent affinities and binding kinetics. Specifically, an *ortho*-methoxy substituent (**12p**) displayed decreased A_{2A}R affinity and RT relative to its *para*-substituted analogue (**12m**), while methyl- (**12o**) or halogen-substituted (**12q**, **12r**) analogues displayed increased A_{2A}R affinities and RT values. For most compounds, disubstitution of the phenylpiperazine did not dramatically change their affinities or binding kinetics (**12t–w**). Interestingly for **12x**, which has *ortho*- and *para*-fluoro substituents, an exceptionally long receptor RT of 323 ± 25 min was found (Table 2) that was

Table 2. Binding affinities and kinetics of compounds **12i–12x**.

						
Compd	R	K_i [nM] ^[a]	k_{on} [nM ⁻¹ ·min ⁻¹] ^[b]	k_{off} [min ⁻¹] ^[b]	RT [min] ^[c]	K_i [nM]
ZM241385	Table 1	0.40 ± 0.03	0.13 ± 0.06	0.014 ± 0.003	71 ± 21	255 ^[23]
12a	4-H	0.30 ± 0.08	0.051 ± 0.005	0.0061 ± 0.0020	164 ± 32	8% ^[d]
12i	4-CH ₃	0.79 ± 0.06	0.062 ± 0.020	0.016 ± 0.006	63 ± 18	14% ^[d]
12j	4-Cl	0.29 ± 0.10	0.090 ± 0.010	0.018 ± 0.006	56 ± 11	35 ± 13
12k	4-CF ₃	0.38 ± 0.10	0.072 ± 0.009	0.020 ± 0.005	50 ± 37	64% ^[d]
12l	4-F	0.54 ± 0.05	0.10 ± 0.02	0.020 ± 0.005	50 ± 8	57% ^[d]
12m	4-OCH ₃	0.51 ± 0.10	0.064 ± 0.005	0.0079 ± 0.0020	127 ± 19	11% ^[d]
12n	4-Ph	1.4 ± 0.2	0.018 ± 0.002	0.034 ± 0.010	29 ± 2	32% ^[d]
12o	2-CH ₃	0.13 ± 0.04	0.062 ± 0.002	0.0075 ± 0.0020	133 ± 21	29% ^[d]
12p	2-OCH ₃	3.5 ± 0.7	0.032 ± 0.003	0.070 ± 0.070	14 ± 11	19% ^[d]
12q	2-Cl	0.13 ± 0.03	0.068 ± 0.016	0.0065 ± 0.0010	154 ± 25	30% ^[d]
12r	2-F	0.12 ± 0.05	0.052 ± 0.012	0.011 ± 0.002	91 ± 15	28% ^[d]
12s	3-F	0.29 ± 0.03	0.055 ± 0.009	0.012 ± 0.003	83 ± 14	62% ^[d]
12t	2,4-diCH ₃	0.16 ± 0.01	0.11 ± 0.02	0.012 ± 0.001	78 ± 9	29% ^[d]
12u	3,4-diCl	0.31 ± 0.10	0.10 ± 0.01	0.015 ± 0.004	67 ± 11	21 ± 4
12v	2,4-diCl	0.15 ± 0.02	0.11 ± 0.01	0.014 ± 0.001	70 ± 5	80 ± 24
12w	2-F, 4-OCH ₃	0.24 ± 0.05	0.054 ± 0.005	0.0083 ± 0.0010	120 ± 65	27% ^[d]
12x	2,4-diF	0.33 ± 0.04	0.034 ± 0.004	0.0031 ± 0.0002	323 ± 25	22% ^[d]

[a] Displacement of specific [³H]ZM241385 binding from the hA_{2A}R at 4 °C. [b] k_{on} and k_{off} values were determined in a competition association assay at 4 °C. [c] RT (residence time) = 1/ k_{off} . [d] Percent displacement of specific [³H]DPCPX binding from the hA₁R at 1 μM at 25 °C. Data are the mean ± SEM of three separate experiments, each performed in duplicate.

much longer than the simple sum of the RT values of the monofluorinated analogues (**12l**, **12r**, and **12s**) and almost fivefold longer than the RT of ZM241385. From Figure 1B, it also follows that **12x** had a much longer RT than ZM241385 (the radioligand), as a typical “overshoot” in specific radioligand binding was observed.^[11] By contrast, if a competitor dissociates faster from its target than the radioligand, the specific binding of the radioligand will slowly and monotonically approach equilibrium over time, as observed for **12c** (Figure 1B).^[11]

Almost all prepared phenylpiperazine triazolo-triazine derivatives displayed high selectivity over the human adenosine A₁ receptor (A₁R), i.e., < 50% of [³H]DPCPX displacement on A₁R at 1 μM (Tables 1 and 2). Notably, the compound with the longest RT toward A_{2A}R, **12x**, had very good A_{2A}R selectivity over the A₁R (Table 2). In contrast, **12j**, **12u**, and **12v**, with mono- or dichloro substitution, lost some selectivity over the A₁R (K_i values at the A₁R ranged from 20 nM to 80 nM, Table 2). Interestingly, all of these compounds contain a chloro substituent

in the *para* position, yet this substituent in other positions (e.g., **12q**, *ortho* substituent) did not exhibit lower selectivity for the A_{2A}R over the A₁R.

Functional characterization of **12x** and **12c** in a cAMP assay

Subsequently, the compounds with the longest and shortest RT with high affinity (i.e., **12x** and **12c**) were functionally characterized in an A_{2A}R agonist-induced cAMP assay, which revealed their antagonistic behavior. Firstly, it follows from Figure 1C that both **12x** and **12c** induced a concentration-dependent decrease of intracellular cAMP levels with 16-fold difference in their IC₅₀ values, which were 1.4 ± 0.1 nM and 21.8 ± 0.5 nM, respectively (Table 3). Secondly, pre-treatment of HEK293 hA_{2A}R cells with different concentrations of **12x** before stimulation with an AR agonist (i.e., 5'-N-ethylcarboxamidoadenosine, NECA) induced insurmountable antagonism (Table 3). In other words, the NECA concentration–effect curve was shifted to the right, with a concomitant decrease in the maximal

Table 3. Functional characterization of **12x** and **12c** in a cAMP assay.

Compd	IC ₅₀ [nM] ^[a]	Pre-incubation ^[a]		Co-incubation ^[a]		Mode of antagonism ^[b]
		pA ₂	Schild slope	pA ₂	Schild slope	
12c	1.4 ± 0.1	8.62 ± 0.29	0.93 ± 0.11	8.57 ± 0.06	0.93 ± 0.02	Competitive surmountable
12x	21.8 ± 0.5	NA	NA	9.69 ± 0.03	1.13 ± 0.01	Competitive insurmountable

[a] Antagonist potency values were determined from concentration–response curves for **12x** and **12c** in the presence of 100 nM NECA with a 30 min co-incubation; antagonists were pre-incubated for 30 min or co-incubated with NECA at concentrations ranging from 100 μM to 0.1 nM. Data are the mean ± SEM of three separate experiments, each performed in duplicate at 22–25 °C. NA: not available. [b] See text for further explanation.

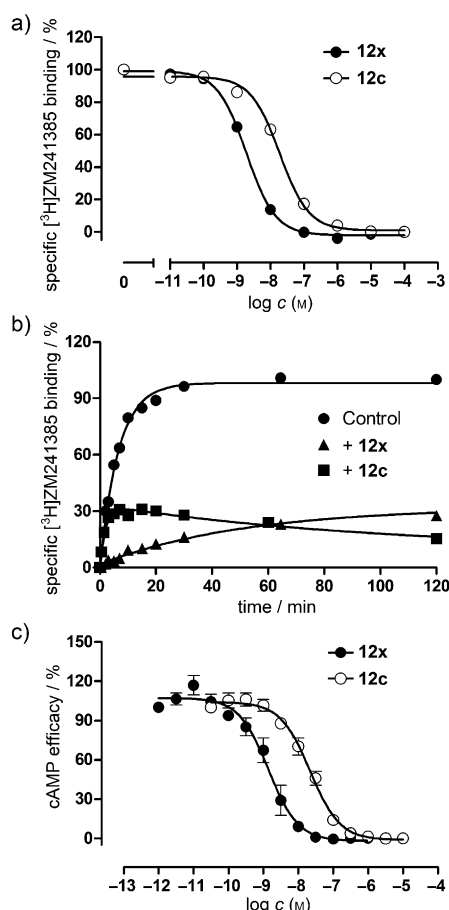


Figure 1. a) Displacement of specific [³H]ZM241385 binding from the hA_{2A} receptor by two representative compounds, namely **12x** and **12c**. b) [³H]ZM241385 competition association binding in the absence of ligand (control) and in the presence of 10×K_i of unlabeled **12x** or **12c**. Data were fitted to the equation described in the Experimental section to calculate the *k*_{on} and *k*_{off} values for unlabeled ligands. Representative graphs are from one experiment performed in duplicate (see Tables 1 and 2 for affinity and kinetic values); c) Concentration–effect curves for **12x** and **12c** in a cAMP assay (percentage relative to 100 μM NECA). Data were obtained by adding HEK293 hA_{2A}R cells to the mixture of the antagonist (**12x** or **12c**) and 100 nM NECA for a 30 min incubation. Data are expressed as mean ± SEM from at least three independent experiments (see Table 3 for potency values).

response (Figure 2A). Conversely, **12c** displayed surmountable A_{2A}R antagonism (Table 3), shifting the NECA curve to the right without affecting its maximal response (Figure 2B). In addition, the pA₂ value for **12c** generated from a Schild plot was 8.62 ± 0.29, which was similar to its pK_i value (8.40 ± 0.10), and the Schild slope was close to unity (0.93 ± 0.11), suggesting that **12c** competed with NECA for the same receptor binding site. To further examine whether **12x** and **12c** both bound to the same site as the agonist, we also performed a co-incubation experiment with **12x** or **12c** in the presence of NECA. It follows from Figure 2C,D that in this experimental setup, both compounds produced a shift to the right in the NECA dose–response curve without suppression of the maximal response, indicative of a competitive interaction. Hence, these findings oppose that insurmountable antagonism resulted from an allo-

steric mode of inhibition, which would be proven by suppression of the maximal response in the co-incubation experiment.^[12] Notably, the generated pA₂ values of **12x** and **12c** in this experimental setup were similar to their pK_i values, and the derived Schild slopes were close to unity (Table 3). Together, this confirmed that **12x** or **12c** bound fully competitively with NECA, and the insurmountable A_{2A}R antagonism of **12x** was a result caused by so-called hemi-equilibrium during the functional assay, due to its long A_{2A}R RT profile.^[12b]

It needs to be pointed out that functional characterization and determination of antagonist binding kinetics were performed at 4 °C and thus do not reflect in vivo RT values, that is, at body temperature. However, it is reasonable to expect that the ranking of the compound RT values at 4 °C will agree with those at higher, more physiological, temperatures. One example at the A_{2A}R is the agonist UK432097, which has previously been shown to have a fivefold longer RT than agonist CGS21680.^[15b] This difference at 4 °C apparently translates into a distinct duration of action in vivo reported by Mantell et al., that is, 8 h for UK432097 and less than 1 h for CGS21680.^[14]

Generation of a kinetics map and physicochemical correlation plots

Next, we plotted an on-/off-rate graph, or “kinetics map”, including the data for all A_{2A}R ligands obtained in this study (Figure 3).^[13] This kinetics map depicted the ligand–receptor binding affinity (*K*_D, represented by parallel diagonal lines) as detailed kinetic rates that reflect the process of target ET (*k*_{on}, y axis) and the target RT (*k*_{off}, x axis), respectively. We observed that the compounds can be divided into three groups: firstly, both the *k*_{on} and *k*_{off} values could vary by one order of magnitude (Figure 3, Group A), while the *K*_D remained within a narrow range (0.1–0.3 nM), as mentioned above. This indicated that compounds with the same affinity may have many different combinations of on- and off-rates, even within the same scaffold and target system. Such information, often ignored or unavailable in traditional SAR studies, can in fact be highly decisive in translating the in vitro profile in of a lead to in vivo pharmacokinetics (PK) and/or pharmacodynamics (PD) behavior.^[14] Secondly, compounds sharing the same off-rate may bear divergent *K*_D values, due to different on-rates (Group B). It has been shown in several cases that a slow compound dissociation rate is pivotal for high in vivo efficacy.^[15] Thus, in retrospect, one could imagine that many compounds with promising *k*_{off} values were overlooked simply due to their low scores in classical affinity- or potency-dominated evaluations. Thirdly, the same holds for a compound's on-rate (Group C), i.e., merely focusing on the *K*_D value of a ligand can result in compounds without the desired on-rate, as exemplified by candidate drugs aimed at acute diseases where a rapid onset of action is desired (e.g., acute respiratory distress syndrome).^[2a,f] Taken together, the kinetics map provides a detailed interpretation of a ligand–receptor binding process with a full inventory of *k*_{on}, *k*_{off} and *K*_D values of a series of compounds.

Molecular and physicochemical properties of the synthesized phenylpiperazine analogues (**12i–x** and **12a**) and their puta-

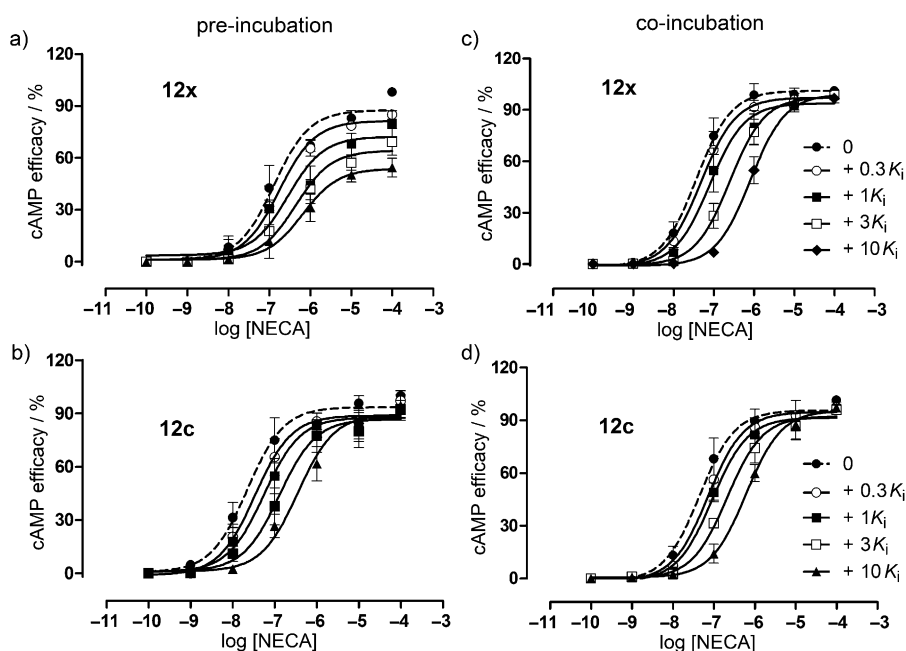


Figure 2. cAMP experiments were performed on HEK293 human embryonic kidney cells stably expressing the $hA_{2A}R$ at room temperature (22–25 °C). a) **12x** or b) **12c** were incubated for 30 min prior to challenge of the adenosine receptor agonist NECA at concentrations ranging from 100 μM to 0.1 nM for another 30 min. c) **12x** or d) **12c** were co-incubated with NECA at concentrations ranging from 100 μM to 0.1 nM for 30 min. The agonist curves were generated in the presence of increasing concentrations of antagonist, namely 0.3-, 1-, 3- and 10-fold their respective K_i values. Data were normalized according to the maximal response produced by 100 μM NECA. The shift in agonist EC_{50} was determined to perform Schild analyses. Data are expressed as mean \pm SEM from at least three independent experiments performed in duplicate.

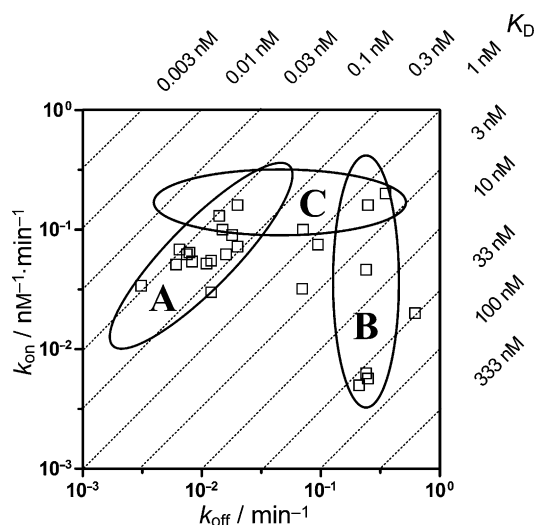


Figure 3. Kinetics map (y axis: k_{on} $nm^{-1} \cdot min^{-1}$; x axis: k_{off} min^{-1}) of all $A_{2A}R$ ligands tested in this study. The kinetically derived affinity ($K_D = k_{off}/k_{on}$) is represented by parallel diagonal lines. Group A: compounds that had varied k_{on} and k_{off} values across several orders of magnitude, while the K_D remained within a similar range (0.1–0.3 nM). Group B: compounds that had the same k_{off} values, but divergent K_D values. Group C: compounds that had the same k_{on} values, but divergent K_D values.

tive relationship with the on- and off-rates were examined in efforts to identify key factor(s) affecting their binding kinetics (Figure 4). As the main scaffold of these series of compounds

is the same, we specifically focused on the properties of C_2 -phenylpiperazine fragments. Several descriptors were selected to be further examined in correlation plots. These included the size (molecular weight, M_r [Da]), surface (molecular surface area, MSA), lipophilicity ($\log P$), and charge (ionization constant, pK_a) of the fragment. There was no obvious linear correlation between the association/dissociation rates and M_r , $\log P$, MSA, or pK_a values. We also performed a multiple linear regression analysis to check whether compound binding kinetics were directed by a combination of two or more of the physicochemical descriptors. However, no significant correlation was found (significance $F > 0.05$ in all cases). Altogether, this indicated that the binding kinetics were compound-specific and that there is no general trend in the correlation of their molecular and physicochemical properties.

Importance of the C_2 -phenylpiperazine fragment and its location

In this study, we observed that, upon minor chemical modifications of the phenylpiperazine side chain on the triazolotriazine scaffold (Tables 1 and 2), binding affinity of the derivatives underwent only subtle changes, while their binding kinetics were very sensitive to such structural variations. For instance, upon substitution of **12a**, **12k** (*para*-trifluoromethyl substituted) displayed a similar K_i value as **12a**, while its off-rate was increased 3.4-fold. In another case, the on- and off-rates of **12u** (*meta*-, *para*-chloro disubstituted) were increased and decreased, respectively, by a similar magnitude (approximately twofold), leading to an unchanged affinity value relative to **12a**. Table 2 as a whole exemplifies the difficulty of selecting a next-stage candidate based on SAR alone. Most compounds have subnanomolar affinity, and compound **12x** does not stand out in any particular way.

The lack of large changes in binding affinities might be expected, given the absence of direct interactions between the phenylhydroxy group and the receptor in a recently determined high-resolution crystal structure of ZM241385-bound $A_{2A}R$.^[17] In this structure, the phenylhydroxy group points away from the binding pocket toward the extracellular space. Likewise, in another crystal structure of UK432097-bound $A_{2A}R$, the bulky tail of agonist UK432097 at the adenine C_2 position extends out of the ligand-binding cavity.^[18] Notably, it was re-

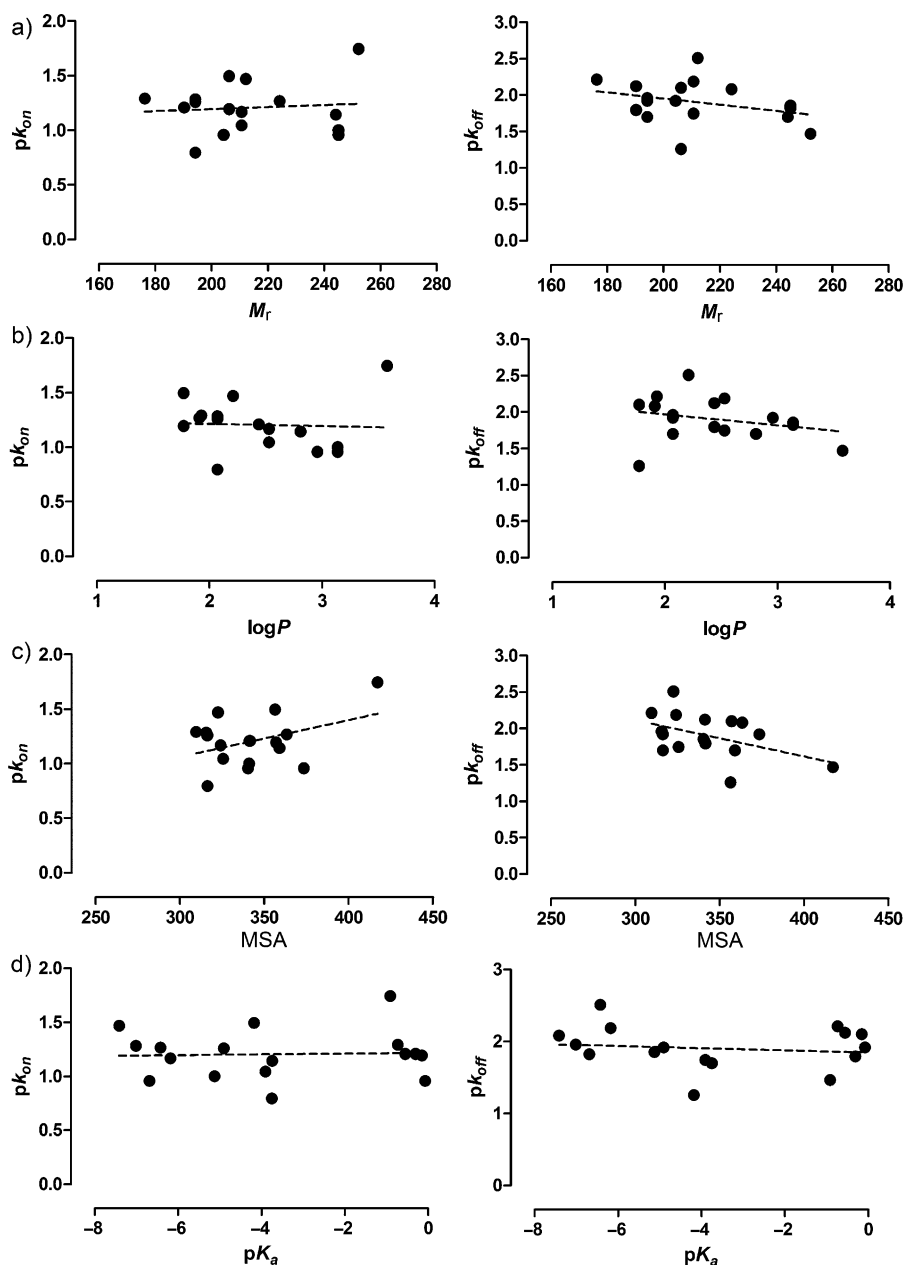


Figure 4. Molecular descriptors of a) size (M_r), b) lipophilicity ($\log P$), c) molecular surface area (MSA, 3D), and d) charge (pK_a) of the substituted C_2 -phenylpiperazine fragments and their correlation with the log values of on- (left side) and off-rates (right side). No clear linear correlation was observed between the association/dissociation rates and M_r (for association: $R^2 = 0.0089$, $P = 0.7180$; for dissociation: $R^2 = 0.1059$, $P = 0.2024$), $\log P$ (for association: $R^2 = 0.0023$, $P = 0.8563$; for dissociation: $R^2 = 0.0731$, $P = 0.2938$), MSA (for association: $R^2 = 0.1629$, $P = 0.1082$; for dissociation: $R^2 = 0.2107$, $P = 0.0638$), or pK_a (for association: $R^2 = 0.0018$, $P = 0.8727$; for dissociation: $R^2 = 0.0187$, $P = 0.6010$).

cently published that this agonist also has a slow association rate and a long RT at the $A_{2A}R$.^[15b] Based on these findings, we postulated that the C_2 -phenylpiperazine group protrudes outward without forming direct interactions with residues in the binding pocket of the triazolotriazine core. Instead, it may interact with residues that are located in the extracellular loops or the adjacent regions of the binding cavity along its trajectory of associating to or dissociating from the receptor. Such reasoning is supported by a recent molecular dynamics simulation

study of the β_1 - and β_2 -adrenergic receptors by Dror et al.^[19] They found that several beta blockers and one beta agonist all traverse the same well-defined, dominant pathway as they bind to the β_1 - and β_2 -adrenergic receptors, initially making contact with a so-called “vestibule” on the receptor’s extracellular surface. Interestingly, this holds true for the ligand binding dynamics of the M_3 muscarinic acetylcholine receptor too. Simulation results indicated that as tiotropium binds to or dissociates from the receptor, it pauses at an alternative binding site in the extracellular vestibule.^[20] Taken together, such an extracellular vestibule appears to play an important role in the on- or off-trajectory to and from the binding pocket of a GPCR.^[19] We therefore assume that the derivatives of ZM241385 also transiently interact with a similar extracellular region of the $A_{2A}R$. This is in accordance with our observation that a change in the C_2 -phenylpiperazine group significantly affected the ligand association and dissociation rates at the $A_{2A}R$, while their K_i values were minimally changed.

Conclusions

We have exemplified an extensive SKR in addition to a traditional SAR analysis at the $A_{2A}R$. Compound **12x**, the high-affinity $A_{2A}R$ ligand previously reported by Vu et al.,^[7c] was revealed to have an exceptionally long RT (323 min). Compared with traditional SAR analysis, such a kinetic insight provided a further ration-

ale to support the selection of **12x** from otherwise chemically and biologically similar compounds for further testing. Kinetics mapping of all tested $A_{2A}R$ ligands also provided a detailed interpretation of the ligand–receptor binding process. Next, a functional comparison between **12c** and **12x** in different assay formats (co-application versus pre-incubation) further revealed competitive insurmountable antagonism of **12x** at the $hA_{2A}R$ —a phenomenon distinct from that of **12c**. In addition, investigation of the molecular properties indicated that the

ligand–receptor binding kinetics were most likely driven by specific interactions between the ligand and the receptor. As an extension of the current study, it would be of great interest to subject compounds having similar affinity yet different binding kinetics to (pre)clinical tests. This would show how relevant the variations in RT and on-/off-rates are in terms of in vivo efficacy and duration of action. We believe that SKR, in combination with traditional SAR, can serve as an important tool for more directed medicinal chemistry efforts in the future.

Experimental Section

Chemical synthesis

General: All solvents and reagents were purchased from commercial sources and were of analytical grade. Demineralized water is simply referred to as H₂O and was used in all cases unless stated otherwise (i.e., brine). ¹H and ¹³C NMR spectra were recorded on a Bruker AV 400 liquid spectrometer (¹H NMR, 400 MHz; ¹³C NMR, 101 MHz) at room temperature. Chemical shifts are reported in parts per million (ppm), are designated by δ , and are downfield of the internal standard tetramethylsilane (TMS). Coupling constants are reported in Hz and are designated as *J*. High-resolution mass spectrometry was performed by the Leiden Institute of Chemistry and recorded by direct injection (2 μ L of a 2 μ M solution in H₂O/CH₃CN; 50:50; v/v and 0.1% formic acid) on a mass spectrometer (Thermo Finnigan LTQ Orbitrap) equipped with an electrospray ion source in positive mode (source voltage 3.5 kV, sheath gas flow 10, capillary temperature 275 °C), with resolution (*R*) = 60 000 at *m/z* 400 (mass range *m/z* = 150–2000) and calibrated for dioctylphthalate (*m/z* = 391.28428). Analytical purity of the final compounds was determined by high performance liquid chromatography (HPLC) with a Phenomenex Gemini 3u C18 110A column (50 \times 4.6 mm, 3 μ m), measuring UV absorbance at 254 nm. Sample preparation and HPLC method were as follows, unless stated otherwise: 0.3–0.8 mg of compound was dissolved in 1 mL of a 1:1:1 mixture of CH₃CN/H₂O/*t*BuOH and eluted from the column within 15 min, with a three-component system of H₂O/CH₃CN/1% TFA in H₂O, decreasing polarity of the solvent mixture over time from 80:10:10 to 90:0:10. All compounds showed a single peak at the designated RT and are at least 95% pure. Thin-layer chromatography (TLC) was routinely consulted to monitor the progress of reactions, using aluminum-coated Merck silica gel F₂₅₄ plates. Purification by column chromatography was achieved by use of Grace Davison Davisil silica column material (LC60A, 30–200 μ m). Solutions were concentrated using a Heidolph Laborota W8 2000 evaporation apparatus and by high vacuum on a Binder APT line vacuum drying oven. The procedure for a series of similar compounds is given as a general procedure for all within that series, annotated by the numbers of the compounds.

2-(Furan-2-carboxamido) guanidine (2): A mixture of hydrazide 1 (0.1 mol, 12.6 g) and *S*-methylisothiurea sulfate (0.05 mol, 13.9 g) in an 1% aqueous NaOH solution (400 mL) was stirred at room temperature for 72 h. The precipitated solid (2), was filtered, washed with ice water, and used in next step without further purification: ¹H NMR (400 MHz, [D₆]DMSO): δ = 10.77 (brs, 1H, NH), 7.56 (s, 1H), 6.88 and 6.76 (2 \times s due to dimer formation, 2H, NH₂), 6.64 (d, *J* = 2.8 Hz, 1H), 6.45 ppm (dd, *J* = 2.0, 0.8 Hz, 1H).

5-(Furan-2-yl)-2H-1,2,4-triazol-3-amine (3): Guanidine 2 (53.6 mmol, 9.0 g) was stirred in a 1:1 mixture of EtOAc/H₂O (400 mL) for 3 h. After extraction with EtOAc (2 \times 150 mL), the or-

ganic layer was washed with H₂O and brine (2 \times 100 mL each) and dried over anhydrous Na₂SO₄. After removing the solvent, 4 was obtained as a white solid (6.51 g, two-step yield: 54%): ¹H NMR (400 MHz, [D₆]DMSO): δ = 12.08 (brs, 1H, NH), 7.68 (s, 1H), 6.67 (s, 1H), 6.54 (s, 1H), 6.08 ppm (s, 2H).

2-(Furan-2-yl)-5-(methylthio)-[1,2,4]triazolo[1,5-*a*][1,3,5]triazin-7-amine (4): A mixture of amine 3 (43.4 mmol, 6.5 g) and dimethyl *N*-cyanodithio(imino)carbonate (47.8 mmol, 7.0 g) was heated at 180 °C in a stream of nitrogen for 4 h, then cooled to room temperature to add 30 mL of a CH₂Cl₂/CH₃OH (1:1) solution. The mixture was stirred at reflux for another 1.5 h, followed by filtration. The solids were washed by the solution, and the solvent was removed under reduced pressure. The residue was purified by column chromatography, eluting with CH₂Cl₂ containing increasing amounts of EtOAc (0–50%). This gave compound 4 as a pale-yellow solid (3.2 g, yield: 30%): ¹H NMR (400 MHz, CD₃OD): δ = 7.91 (dd, *J* = 1.7, 0.7 Hz, 1H), 7.12 (dd, *J* = 3.4, 0.7 Hz, 1H), 6.70 (dd, *J* = 3.4, 1.7 Hz, 1H), 2.55 ppm (s, 3H).

2-(Furan-2-yl)-5-(methylsulfonyl)-[1,2,4]triazolo[1,5-*a*][1,3,5]triazin-7-amine (5): A solution of *m*CPBA (70%, 32.5 mmol, 8.0 g) in CH₂Cl₂ (20 mL) was added to a stirred, ice-cooled suspension of the sulfide (R = MeSO) (13.0 mmol, 3.2 g) in CH₂Cl₂ (50 mL). The resulting solution was stirred overnight (0 °C \rightarrow room temperature). The solvent was removed, and EtOH (70 mL) was added to the residue. The solid was collected by filtration, washed with EtOH, and dried in a vacuum oven to give a white solid (R = MeSO₂) (yield: 3.2 g, 88%): ¹H NMR (400 MHz, [D₆]DMSO): δ = 9.81 and 9.48 (2 \times s due to dimer formation,^[8c] 2H, NH₂), 7.98 (dd, *J* = 1.2, 0.8 Hz, 1H), 7.34 (dd, *J* = 2.4, 0.8 Hz, 1H), 6.73 (dd, *J* = 2.4, 1.2 Hz, 1H), 3.35 ppm (s, 3H).

1-(2,4-Dichlorophenyl)piperazine (9v): A mixture of 6 (16.7 mmol, 2.0 mL) and piperazine (83.6 mmol, 7.2 g) in 10 mL of *N,N*-dimethylacetamide was heated in the microwave at 165 °C for 6.5 h, after which 6 was consumed, as shown by TLC. H₂O and CH₂Cl₂ were added, and the pH value was adjusted to 1 with 1 M HCl_(aq). The aqueous layer was washed three times with CH₂Cl₂ and subsequently brought to pH 12 with 5 M NaOH_(aq). After extraction of the basified aqueous layer with CH₂Cl₂, the combined organic layers were washed four times with H₂O, dried over MgSO₄, and concentrated in vacuo to yield 9v as a yellow oil (yield: 2.4 g, 61%): ¹H NMR (400 MHz, CDCl₃): δ = 7.36 (d, *J* = 2.4 Hz, 1H), 7.19 (dd, *J* = 8.8, 2.4 Hz, 1H), 6.95 (d, *J* = 8.4 Hz, 1H), 3.06–3.02 (m, 5H, 2 \times CH₂ and NH), 2.99–2.96 ppm (m, 4H).

1-(2-Fluoro-4-methoxyphenyl)piperazine hydrochloride (9w): A mixture of bis(2-chloroethyl)amine hydrochloride (9.59 mmol, 1.7 g) (7) and 1-BuOH (20 mL) was treated slowly with 2-fluoro-4-methoxybenzenamine (9.14 mmol, 1.3 g) at room temperature. After the addition, the mixture was stirred at reflux for 48 h and then cooled. The solid was filtered and rinsed with CH₃OH and Et₂O to give 9w as a white solid (yield: 660 mg, 29%): ¹H NMR (400 MHz, CDCl₃): δ = 9.21 (brs, 2H, NH, and HCl), 7.07–7.02 (m, 1H), 6.86–6.83 (m, 1H), 6.74–6.71 (m, 1H), 3.72 (s, 3H), 3.28–3.20 (m, 4H), 3.14–3.10 ppm (m, 4H).

1-(2,4-Difluorophenyl)piperazine (9x): A mixture of piperazine (24.9 mmol, 2.14 g), 1-bromo-2,4-difluorobenzene (8) (4.1 mmol, 0.8 g), *t*BuONa (5.8 mmol, 0.56 g), BINAP (0.25 mmol, 0.16 g), and Pd₂(dba)₃ (0.083 mmol, 0.048 g) in dry toluene was heated at 110 °C under a nitrogen atmosphere for 24 h. The mixture was filtered over Celite and rinsed with CH₂Cl₂. The solution was washed with H₂O and brine (2 \times 10 mL each), dried over Na₂SO₄, and the solvent was evaporated in vacuo. The residue was purified by silica

gel via $\text{CH}_2\text{Cl}_2/\text{CH}_3\text{OH}$ (10:1) to give compound **9x** as a pale-yellow oil (yield: 337 mg, 42%): ^1H NMR (400 MHz, CDCl_3): δ = 6.91–6.87 (m, 1H), 6.83–6.78 (m, 2H), 3.06 (t, J = 3.6 Hz, 4H), 3.00–2.97 (m, 4H), 1.80 ppm (s, 1H, NH).

General procedure for the preparation of compounds 10a–d and 10i–x: A mixture of the appropriate phthalimide-protected alkyl bromide (7.5 mmol), piperazine derivative (5 mmol) and K_2CO_3 (10 mmol) in DMF (5 mL) was stirred at 70 °C overnight. The reaction mixture was cooled, washed with H_2O (5 mL), and extracted with EtOAc (3 × 10 mL each). The organic phase was then combined, dried over Na_2SO_4 , and evaporated in vacuo to give the crude product, which was recrystallized from EtOH and/or CH_3OH or purified by chromatography (petroleum ether/EtOAc).

2-(2-(4-Phenylpiperazin-1-yl)ethyl)isoindoline-1,3-dione (10a): Compound **10a** was obtained as a pale-yellow solid after column chromatography with petroleum ether/EtOAc (5:1–1:1) (yield: 1.5 g, 43%): ^1H NMR (400 MHz, CDCl_3): δ = 7.86–7.80 (m, 4H), 7.25–7.24 (m, 2H), 6.91–6.88 (m, 2H), 6.80 (t, J = 8.1 Hz, 1H), 3.87 (t, J = 6.3 Hz, 2H), 3.15–3.12 (m, 4H), 2.72–2.68 ppm (m, 6H).

General procedure for preparation of compounds 11a–d and 11i–x: An excess of hydrazine hydrate was added (1–5 mL) to a solution of isoindoline-1,3-dione (3 mmol) in EtOH (25 mL), and the mixture was stirred at 70 °C overnight. The solvent was removed in vacuo, and EtOAc was added to the residue. The solids were filtered, dried over Na_2SO_4 , and the solvent was evaporated in vacuo to give the crude product as a pale-yellow oil or solid. The crude product was used in the next step without further purification.

General procedure for preparation of compounds 12a–x: A mixture of the respective amine (0.75 mmol), the sulfone/sulfoxide mixture (**5**) (0.50 mmol), and Et_3N (1.0 mmol) was dissolved in CH_3CN and stirred at reflux overnight. After removing the solvent in vacuo, EtOAc was added, and the organic phase was washed with H_2O and brine (2 × 10 mL each), dried over Na_2SO_4 , and evaporated. The residue was purified by column chromatography using silica gel and EtOAc or EtOAc/ CH_3OH to afford a white or off-white solid.

2-(Furan-2-yl)-N5-(2-(4-phenylpiperazin-1-yl)ethyl)-[1,2,4]triazolo-[1,5-a][1,3,5]triazine-5,7-diamine (12a): Eluting with EtOAc/ CH_3OH (10:1) afforded the title compound as a white powder (yield: 55 mg, 14%): ^1H NMR (400 MHz, MeOD): δ = 7.68 (s, 1H), 7.22 (t, J = 8.4 Hz, 2H), 7.12 (d, J = 3.2 Hz, 1H), 6.96 (d, J = 8.4 Hz, 2H), 6.84–6.81 (m, 1H), 6.60 (d, J = 1.6 Hz, 1H), 3.61–3.60 (m, 2H), 3.20 (t, J = 4.8 Hz, 4H), 2.72 (t, J = 4.8 Hz, 4H), 2.68–2.67 ppm (m, 2H). ^{13}C NMR (101 MHz, $[\text{D}_6]\text{DMSO}$): δ = 161.6, 159.7, 156.3, 151.5, 150.5, 146.7, 145.1, 129.4, 119.2, 115.8, 112.4, 112.1, 57.1, 53.2, 48.7, 38.5 ppm. HRMS (ESI) m/z $[\text{M}+\text{H}]^+$ calcd for $\text{C}_{20}\text{H}_{24}\text{N}_9\text{O}^+$: 406.2026, found: 406.2092; HPLC: t_{R} = 11.96 min, purity = 96.7%.

Pharmacological characterization

Materials: $[\text{^3H}]\text{ZM241385}$ (specific activity 50 Ci mmol $^{-1}$) and $[\text{^3H}]\text{1,3-dipropyl-8-cyclopentyl-xanthine}$ ($[\text{^3H}]\text{DPCPX}$, specific activity 116.7 Ci mmol $^{-1}$) were purchased from ARC Inc. (St. Louis, USA). Unlabeled ZM241385 was a gift from Dr. S. M. Poucher (AstraZeneca, Macclesfield, UK). CGS21680 was a gift from Dr. R. A. Lovell (Ciba-Geigy, Summit, NJ). NECA (5'-N-ethylcarboxamidoadenosine) and DPCPX were purchased from Sigma-Aldrich (Steinheim, Germany). Adenosine deaminase (ADA) was purchased from Boehringer Mannheim (Mannheim, Germany). Bicinchoninic acid (BCA) and BCA protein assay reagent were obtained from Pierce Chemical Company (Rockford, IL, USA). Human embryonic kidney cells stably

expressing the $\text{hA}_{2\text{A}}\text{R}$ (HEK293 $\text{hA}_{2\text{A}}\text{R}$) were kindly provided by Dr. J. Wang (Biogen/IDEC, Cambridge, MA). Chinese hamster ovary cells stably expressing the hA_1R (CHO hA_1R) were kindly provided by Prof. Steve Hill (University of Nottingham, UK). All other chemicals were of analytical grade and obtained from standard commercial sources.

Cell culture and membrane preparation: Cell culture and membrane preparation were performed as reported previously.^[15b,21]

Radioligand displacement assay: Radioligand displacement from the hA_1R and $\text{hA}_{2\text{A}}\text{R}$ was determined using the displacement assay as described previously.^[15b,21]

Radioligand competition association assay: The binding kinetics of unlabeled $\text{A}_{2\text{A}}\text{R}$ ligands were determined at 4 °C using the competition association assay as described previously.^[15b]

cAMP assay: HEK293 $\text{hA}_{2\text{A}}\text{R}$ cells were cultured as a monolayer on 10 cm ϕ culture plates to 80%–90% confluency. Cells were harvested and centrifuged two times at 200 × g for 5 min. The amount of cAMP produced was determined with the LANCE ultra cAMP 384 kit (PerkinElmer, Groningen, Netherlands). In general, 1000 cells per well were seeded on 384-well plates and incubated at room temperature (22–25 °C). cAMP was generated in the stimulation buffer [*N*-2-hydroxyethylpiperazine-*N'*-ethanesulfonic acid (HEPES), 5 mM; 0.1% (w/v) BSA; cilostamide, 50 μM ; rolipram, 50 μM ; adenosine deaminase (ADA), 0.8 IU mL $^{-1}$] Concentration–effect curves for **12x** and **12c** were obtained by adding HEK293 $\text{hA}_{2\text{A}}\text{R}$ cells to a mixture of antagonist (**12x** or **12c**) and 100 nM NECA (prepared in the stimulation buffer) for a 30 min co-incubation. For assessment of either surmountable or insurmountable behavior, the antagonists (**12x** and **12c**) were pre-incubated for 30 min or co-incubated with the agonist NECA at concentrations ranging from 100 μM to 0.1 nM for a duration of 30 min, with antagonist concentrations of 0.3-, one-, two- and tenfold their respective K_i values. The incubation was stopped by adding detection mix and antibody solution, according to the instructions of the manufacturer. The generated fluorescence intensity was quantified on an EnVision Multilabel Reader (PerkinElmer, Groningen, Netherlands). The resulting data were normalized according to the maximal response produced by 100 μM NECA. The shift in agonist EC_{50} was determined to perform Schild analyses.

Data analysis: All experimental data was analyzed using GraphPad Prism 5.0 (GraphPad Software Inc., San Diego, CA). K_D and B_{max} values of $[\text{^3H}]\text{ZM241385}$ at $\text{hA}_{2\text{A}}\text{R}$ membranes were obtained from Guo et al.^[15b] IC_{50} values obtained from competition displacement binding data were converted into K_i values using the Cheng–Prusoff equation.^[22] Association and dissociation rates for unlabeled ligands were calculated by fitting the data in the competition association model using kinetics of competitive binding:^[11]

$$K_A = k_1[L] + k_2 \quad (1)$$

$$K_B = k_3[L] + k_4 \quad (2)$$

$$S = \sqrt{[(K_A - K_B)^2 + 4 \cdot k_1 \cdot k_3 \cdot L \cdot I]} \quad (3)$$

$$K_F = 0.5 (K_A + K_B + S) \quad (4)$$

$$K_S = 0.5 (K_A + K_B - S) \quad (5)$$

$$Q = B_{\text{max}} \cdot k_1 \cdot L \cdot (K_F - K_S)^{-1} \quad (6)$$

$$Y = Q \cdot [k_4 \cdot (K_F - K_S) \cdot K_F^{-1} \cdot K_S^{-1} + (k_4 - K_F) \cdot K_F^{-1} \cdot e^{-K_F \cdot X} - (K_4 - K_S) \cdot K_S^{-1} \cdot e^{-K_S \cdot X}] \quad (7)$$

Where X is the time (min), Y is the specific [^3H]ZM241385 binding (DPM), k_1 and k_2 are the k_{on} ($\text{nm}^{-1}\cdot\text{min}^{-1}$) and k_{off} (min^{-1}) values of [^3H]ZM241385 obtained from Guo et al.,^[15b] L is the concentration of [^3H]ZM241385 used (nM), B_{max} is the total binding (DPM), and I is the concentration of unlabeled ligand (nM). Fixing these parameters allows the following parameters to be calculated: k_3 , which is the k_{on} value ($\text{nm}^{-1}\cdot\text{min}^{-1}$) of the unlabeled ligand, and k_4 , which is the k_{off} value (min^{-1}) of the unlabeled ligand. Molecular property descriptors (M_r , $\log P$, MSA, pK_a) of the substituted C_2 -phenylpiperazine were calculated using MarvinSketch 5.11 (ChemAxon, Hungary). (Multiple) Linear regression analysis was done using Microsoft Excel 2003.

Acknowledgements

The authors thank Dr. Ron Dror and Dr. Albert Pan (D. E. Shaw Research, USA) for fruitful discussions, and Dr. Julien Louvel and Mr. Maris Vilums for helpful comments on the manuscript. This project was supported financially by the Innovational Research Incentive Scheme of the Netherlands Research Organization (NWO; VENI-Grant 11188 to L.H.).

Keywords: binding kinetics • G protein-coupled receptors • antagonism • structure–activity relationships • structure–kinetics relationships

- [1] a) R. Zhang, F. Monsma, *Expert Opin. Drug Discovery* **2010**, *5*, 1023–1029; b) R. A. Copeland, D. L. Pompliano, T. D. Meek, *Nat. Rev. Drug Discovery* **2006**, *5*, 730–739; c) D. C. Swinney, *Nat. Rev. Drug Discovery* **2004**, *3*, 801–808; d) D. C. Swinney, *Lett. Drug Des. Discovery* **2006**, *3*, 569–574; e) S. Núñez, J. Venhorst, C. G. Kruse, *Drug Discovery Today* **2012**, *17*, 10–22.
- [2] a) E. M. Rosethorne, R. J. Turner, R. A. Fairhurst, S. J. Charlton, *Naunyn-Schmiedeberg's Arch. Pharmacol.* **2010**, *382*, 255–263; b) C. C. Govern, M. K. Paczosa, A. K. Chakraborty, E. S. Huseby, *Proc. Natl. Acad. Sci. USA* **2010**, *107*, 8724–8729; c) J. Foote, H. N. Eisen, *Proc. Natl. Acad. Sci. USA* **1995**, *92*, 1254–1256; d) G. Schreiber, *Curr. Opin. Struct. Biol.* **2002**, *12*, 41–47; e) T. Selzer, S. Albeck, G. Schreiber, *Nat. Struct. Biol.* **2000**, *7*, 537–541; f) D. A. Sykes, M. R. Dowling, J. Leighton-Davies, T. C. Kent, E. Renard, A. Trifilieff, S. J. Charlton, *J. Pharmacol. Exp. Ther.* **2012**, *343*, 520–528.
- [3] B. B. Fredholm, A. P. IJzerman, K. A. Jacobson, J. Linden, C. E. Müller, *Pharmacol. Rev.* **2011**, *63*, 1–34.
- [4] K. A. Jacobson, Z. G. Gao, *Nat. Rev. Drug Discovery* **2006**, *5*, 247–264.
- [5] a) B. C. Shook, P. F. Jackson, *ACS Chem. Neurosci.* **2011**, *2*, 555–567; b) C. E. Müller, K. A. Jacobson, *Biochim. Biophys. Acta Biomembr.* **2011**, *1808*, 1290–1308; c) U. Shah, R. Hodgson, *Curr. Opin. Drug Discov. Devel.* **2010**, *13*, 466–480.
- [6] a) S. M. Poucher, J. R. Keddie, P. Singh, S. M. Stoggall, P. W. Caulkett, G. Jones, M. G. Coll, *Br. J. Pharmacol.* **1995**, *115*, 1096–1102; b) P. W. R. Caulkett, G. Jones, M. G. Collis, S. M. Poucher, (Imperial Chemical Industry PLC, London, UK), European Patent No. EP459702, **1991**.
- [7] a) C. B. Vu, D. Pan, B. Peng, G. Kumaravel, G. Smits, X. Jin, D. Phadke, T. Engber, C. Huang, J. Reilly, S. Tam, D. Grant, G. Hetu, R. C. Petter, *J. Med. Chem.* **2005**, *48*, 2009–2018; b) C. B. Vu, B. Peng, G. Kumaravel, G. Smits, X. Jin, D. Phadke, T. Engber, C. Huang, J. Reilly, S. Tam, D. Grant, G. Hetu, R. C. Petter, *J. Med. Chem.* **2004**, *47*, 4291–4299; c) C. B. Vu, P. Shields, B. Peng, G. Kumaravel, X. Jin, D. Phadke, J. Wang, T. Engber, E. Ayyub, R. C. Petter, *Bioorg. Med. Chem. Lett.* **2004**, *14*, 4835–4838.
- [8] a) A. V. Dolzhenko, A. V. Dolzhenko, W. K. Chui, *Tetrahedron* **2007**, *63*, 12888–12895; b) A. V. Dolzhenko, G. Pastorin, A. V. Dolzhenko, W. K. Chui, *Tetrahedron Lett.* **2009**, *50*, 2124–2128; c) M. Jörg, M. Agostino, E. Yuriev, F. S. Mak, N. D. Miller, J. M. White, P. J. Scammells, B. Capuano, *Struct. Chem.* **2013**, *24*, 1241–1251; d) M. Jörg, J. Shonberg, F. S. Mak, N. D. Miller, E. Yuriev, P. J. Scammells, B. Capuano, *Bioorg. Med. Chem. Lett.* **2013**, *23*, 3427–3433.
- [9] P. W. R. Caulkett, G. Jones, M. McPartlin, N. D. Renshaw, S. K. Stewart, B. Wright, *J. Chem. Soc. Perkin Trans. 1* **1995**, 801–808.
- [10] a) R. E. Tenbrink (Pharmacia & Upjohn Company, MI, USA), US Patent No. US5912246, **1999**; b) G. E. Martin, R. J. Elgin, Jr., J. R. Mathiasen, C. B. Davis, J. M. Kesslick, W. J. Baldy, R. P. Shank, D. L. DiStefano, C. L. Fedde, M. K. Scott, *J. Med. Chem.* **1989**, *32*, 1052–1056; c) S. Morita, K. Kitano, J. Matsubara, T. Ohtani, Y. Kawano, K. Otsubo, M. Uchida, *Tetrahedron* **1998**, *54*, 4811–4818.
- [11] H. J. Motulsky, L. C. Mahan, *Mol. Pharmacol.* **1984**, *25*, 1–9.
- [12] a) G. Vauquelin, I. Van Liefde, P. Vanderheyden, *Trends Pharmacol. Sci.* **2002**, *23*, 514–518; b) T. Kenakin, S. Jenkinson, C. Watson, *J. Pharmacol. Exp. Ther.* **2006**, *319*, 710–723; c) G. Vauquelin, A. Szczuka, *Neurochem. Int.* **2007**, *51*, 254–260.
- [13] a) D. A. Sykes, M. R. Dowling, S. J. Charlton, *Mol. Pharmacol.* **2009**, *76*, 543–551; b) D. Guo, T. Mulder-Krieger, A. P. IJzerman, L. H. Heitman, *Br. J. Pharmacol.* **2012**, *166*, 1846–1859.
- [14] a) S. J. Mantell, P. T. Stephenson, S. M. Monaghan, G. N. Maw, M. A. Trevethick, M. Yeadon, R. F. Keir, D. K. Walker, R. M. Jones, M. D. Selby, D. V. Batchelor, S. Rozze, H. Chavarroche, T. J. Hobson, P. G. Dodd, A. Lemaître, K. N. Wright, E. F. Stuart, *Bioorg. Med. Chem. Lett.* **2008**, *18*, 1284–1287; b) S. J. Mantell, P. T. Stephenson, S. M. Monaghan, G. N. Maw, M. A. Trevethick, M. Yeadon, D. K. Walker, M. D. Selby, D. V. Batchelor, S. Rozze, H. Chavarroche, A. Lemaître, K. N. Wright, L. Whitlock, E. F. Stuart, P. A. Wright, F. Macintyre, *Bioorg. Med. Chem. Lett.* **2009**, *19*, 4471–4475.
- [15] K. Andersson, R. Karlsson, S. Lofas, G. Franklin, M. D. Hamalainen, *Expert Opin. Drug Discovery* **2006**, *1*, 439–446.
- [16] J. Gabrielsson, H. Dolgos, P. G. Gillberg, U. Bredberg, B. Benthem, G. Duker, *Drug Discovery Today* **2009**, *14*, 358–372.
- [17] W. Liu, E. Chun, A. A. Thompson, P. Chubukov, F. Xu, V. Katritch, G. W. Han, C. B. Roth, L. H. Heitman, A. P. IJzerman, V. Cherezov, R. C. Stevens, *Science* **2012**, *337*, 232–236.
- [18] F. Xu, H. Wu, V. Katritch, G. W. Han, K. A. Jacobson, Z. G. Gao, V. Cherezov, R. C. Stevens, *Science* **2011**, *332*, 322–327.
- [19] R. O. Dror, A. C. Pan, D. H. Arlow, D. W. Borhani, P. Maragakis, Y. Shan, H. Xu, D. E. Shaw, *Proc. Natl. Acad. Sci. USA* **2011**, *108*, 13118–13123.
- [20] A. C. Kruse, J. Hu, A. C. Pan, D. H. Arlow, D. M. Rosenbaum, E. Rosemond, H. F. Green, T. Liu, P. S. Chae, R. O. Dror, D. E. Shaw, W. I. Weis, J. Wess, B. K. Kobilka, *Nature* **2012**, *482*, 552–556.
- [21] D. Guo, E. J. van Dorp, T. Mulder-Krieger, J. P. van Veldhoven, J. Brussee, A. P. IJzerman, L. H. Heitman, *J. Biomol. Screening* **2013**, *18*, 309–320.
- [22] Y. Cheng, W. H. Prusoff, *Biochem. Pharmacol.* **1973**, *22*, 3099–3108.
- [23] E. Ongini, S. Dionisotti, S. Gessi, E. Irenius, B. B. Fredholm, *Naunyn-Schmiedeberg's Arch. Pharmacol.* **1999**, *359*, 7–10.

Received: November 21, 2013

Revised: January 27, 2014

Published online on March 3, 2014